

Design of permanent magnet synchronous machine for micro-hybrid electric vehicle operation

Abstract. The paper presents characteristics of a permanent magnet synchronous machine designed for micro-hybrid electric vehicle operation. Appropriate design of interior permanent magnet machine with 36 stator slots and 8 stator poles for operation in motor and generator mode was investigated. Finite element analysis is employed in order to determine the machine performance.

Streszczenie. W artykule zaprezentowano charakterystyki działania maszyny synchronicznej z magnesami trwałymi zaprojektowanej dla mikrohybrydowego pojazdu elektrycznego. Przebadano projekt wnętrza, wspomnianej wyżej, maszyny z 36 żłobkami stojana i 8 biegunami w stojanie. Model komputerowy został oparty o metodę elementów skończonych. (Projekt maszyny synchronicznej z magnesami trwałymi dla mikrohybrydowego pojazdu elektrycznego)

Keywords: synchronous machine, permanent magnets, micro-hybrid electric vehicle.

Słowa kluczowe: maszyna synchroniczna, trwały magnes, mikrohybrydowy pojazd elektryczny

Introduction

In general, the hybrid electric vehicle should benefit from the best features of both conventional ICE (internal combustion engine) vehicle and electric vehicle. According to the grade of hybridization the micro, mild and full hybrid configurations are known. Each grade of hybridization of hybrid electric vehicles demands quite a different role of electric machine as well. In micro-hybrids systems electric machines should exhibit start/stop, alternator and sometimes regenerative breaking functions, while electric machine normally does not supply additional torque when the hybrid electric vehicle is cruising. Compared to the conventional vehicles, micro hybrid systems allows in city driving up to 5-10% fuel savings.

Side-mounted belt-driven starter-generator architecture is presented in this paper. The electric machine has to enable starting the ICE and to develop additional torque during acceleration of the vehicle for a short time, typically lower than 5-8 s.

The torque demand about 120 Nm is required in order to crank the engine (assuming 3:1 gear ratio using the belt drive, the corner motor speed with maximal torque in the motor operation mode is around 1500 rpm). Above the corner speed in the motor operation mode, the torque demand is inversely decreasing with increasing of speed. After certain speed the electric machine has to transit from motor to generator mode of operation smoothly (typical transition speed is around 2000 rpm at the ICE side). The electric machine used for starter-generator has to enable regenerative breaking as well, where the maximal regenerative breaking torque value is similar to the maximal torque value in the motor operation mode. Practically all known electric machines can be used as starter-generators, however, induction and permanent magnet machines are frequently used [1-7, 12]. Design of electric machine for starter-generator application, however, does not represent a straightforward and easy task. There are several limitations that should be carefully taken into account during the machine design, as for example: maximum and minimum battery voltage, maximal charging voltage, maximal and nominal continuous charging and discharging current, cooling conditions and used cooling media for the machine, torque and current control of the machine, battery power management, battery cooling capability, etc.

According to all mentioned limitations, the interior permanent magnet machine has been selected for this study, primarily due to the high efficiency in generator mode of operation and good flux weakening possibility [14, 15].

The results for the interior permanent magnet machine with 36 stator slots and 8 rotor poles in the motor and generator operation mode (outer stator diameter of 130 mm, inner stator diameter of 80 mm, active axial length of the machine 90 mm, NdFeB permanent magnets and liquid stator cooling) are presented in this paper. Machine characteristics were calculated by using 2D finite element method software by taking into account copper loss, iron core losses and friction and windage losses as well.

Main PM machine system data are presented in Table I.

Table I. PM MACHINE SYSTEM DATA

	Unit	Value
Stator diameter	(mm)	130
Rotor diameter	(mm)	79
One-side air-gap length	(mm)	0.5
Stack length	(mm)	90
Stator slot number		36
Stator slot area	(mm ²)	85
Pole number		8
Phase number		3
Winding type		double layer
Winding insulation class		F
Winding fill factor		0.37
Number of conductors in slot		8
Number of parallel circuits		4
Phase resistance	(mΩ)	5.139 at 20° Cels.
Stator iron material		M 250-35A
Rotor iron material		M 250-35A
PM material (NdFeB)		Vacodyn 677AP
PM residual flux density	(T)	1.13 at 20° Cels.
PM width	(mm)	22.8
PM height	(mm)	3.5
Maximal battery voltage	(V)	56
Nominal battery voltage	(V)	48
Minimum battery voltage	(V)	30
Motor nominal power	(kW)	3.6
Motor nominal torque	(Nm)	25
Motor peak torque	(Nm)	40
Motor peak power	(kW)	7.2

Method of analysis

The calculation of magnetic conditions:

To obtain the field distributions and the loci of local flux density vectors in the motor, a series of magneto-static field calculations for a complete cycle of field variation was computed by 2D FEM, using the basic equation:

$$(1) \quad \text{rot}(\nu \text{rot}(\mathbf{A})) = \mathbf{J}_0 + \text{rot} \mathbf{M}$$

where ν denotes the reluctivity, \mathbf{A} is the magnetic vector potential, \mathbf{J}_0 is the current density and \mathbf{M} is the magnetization of the permanent magnets.

The non-linearity of the used iron core material was accounted for with a single-valued B - H curve, although more sophisticated models for description of iron core material could be used [8-11]. The magnetic conditions over a complete cycle of magnetic field variation were calculated in 90 discrete equidistant time steps by shifting the rotor position and simultaneously changing the stator excitation.

Terminal voltage and input power calculation:

The discrete time forms of phase voltages were calculated from the average values of the vector magnetic potential in stator slots according to the winding arrangement scheme. The end winding contribution was taken into consideration with the constant value of end winding inductance L_e .

The instantaneous value of the phase voltage in the winding of phase a is given by

$$(2) \quad v_a(t) = Ri_a(t) + \frac{p}{c} \frac{d\psi_{ap}(t)}{dt} + L_e \frac{di_a(t)}{dt}$$

where R is phase resistance, ψ_{ap} is the instantaneous flux linkage of the a phase winding per pole, p is the number of pole pairs and c is the number of parallel circuit of the phase winding. Terminal line-to-line voltage was calculated from calculated waveforms of phase voltages.

The input power was calculated from calculated time forms of phase voltages and the known form of input current as

$$(3) \quad P_i = \frac{1}{T_o} \int [v_a(t)i_a(t) + v_b(t)i_b(t) + v_c(t)i_c(t)] dt$$

The iron loss calculation:

An arbitrary flux density vector variation in each element of mesh was expanded into a Fourier series of elliptical harmonic flux density vectors. The total core loss in the each element of mesh was determined as the sum of total hysteresis losses p_{th} , total classical eddy current losses p_{te} and total excess losses p_{ta} [12-16].

Efficiency determination:

Efficiency in motor and generator mode of operation was determined by the following equations:

$$(4) \quad \eta_{\text{mot}} = \frac{T_{el}\omega_{\text{mec}} - P_{fe} - P_{fw}}{T_{el}\omega_{\text{mec}} + P_{cu}}$$

$$(5) \quad \eta_{\text{gen}} = \frac{T_{el}\omega_{\text{mec}} - P_{cu}}{T_{el}\omega_{\text{mec}} + P_{fe} + P_{fw}}$$

where T_{el} is electromagnetic torque, ω_{mec} is shaft angular speed, P_{cu} are joule losses, P_{fe} are iron core losses and P_{fw} are friction and windage losses.

Results and discussion

Flux distribution over machine cross-section in motor operation mode for: (a) no-load case with only PM excitation, (b) maximal torque mode of operation and (c) maximal flux-weakening is presented in Fig. 1.

Calculated phase and line-to-line back-EMF waveforms are presented in Fig. 2, while the direct-axis and quadrature-axis flux-linkage characteristics in dependency on direct and quadrature-axis current component are presented in Figs. 3-5.

Length of flux-linkage vector for different RMS values of stator current in dependency on rotor position presented in Fig. 5 is a merit for flux-weakening capability of the machine. From Fig. 5 it can be seen that characteristic phase current for optimal flux-weakening capability is 200 A. For lower and higher RMS values of phase current than 200 A, the zero length of flux-linkage vector at maximal flux-weakening cannot be obtained.

Electromagnetic torque profile versus torque angle and electromagnetic torque variation in dependency on rotor position at different RMS values of stator current (current densities in stator slot conductors) are presented in Figs. 6-8. From the results presented in Fig. 7 it can be seen that presented machine exhibits small torque ripple (3%-4.5%) even at very high current densities.

Calculated torque and power characteristics in motor and generator mode of operation are presented in Figs. 9-11. All presented characteristics are determined for the case of pure sinusoidal current supply with minimal, nominal and maximal battery voltage taken into account. Variation of friction and windage losses in dependency on speed (friction and windage losses were obtained from the experiments on the similar size machine) was taken into account by determination of machine efficiency as well.

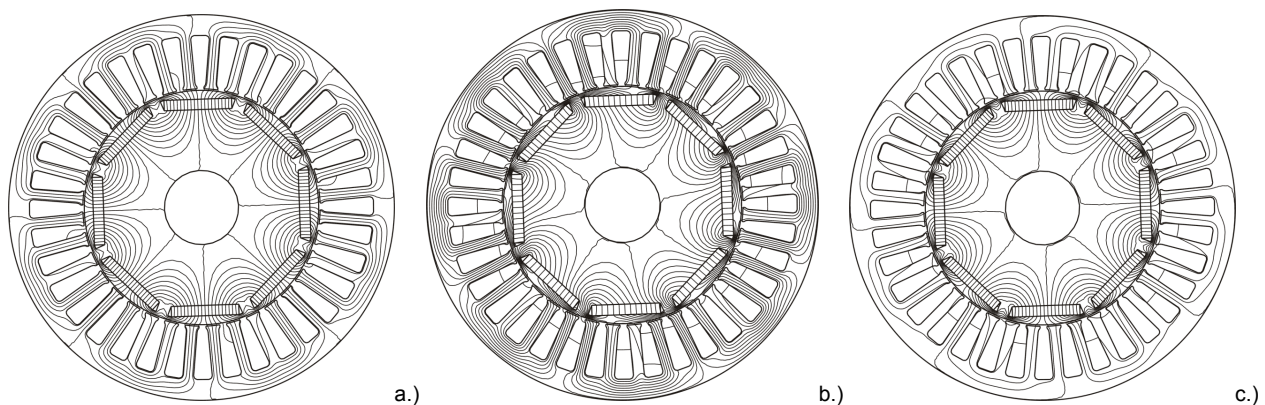


Fig. 1. Flux distribution over machine cross-section in motor operation mode: (a) no-load case, only PM excitation; (b) maximal torque; (c) maximal flux-weakening

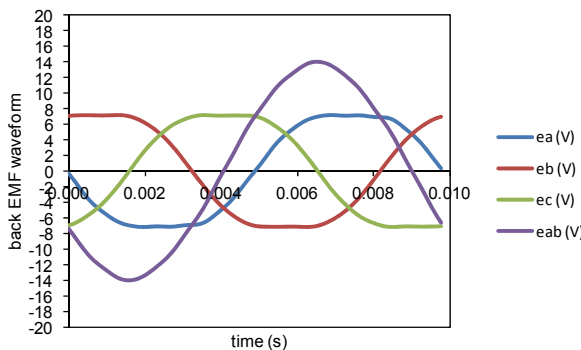


Fig. 2. Phase and line-to-line back EMF waveform at 1500 rev/min

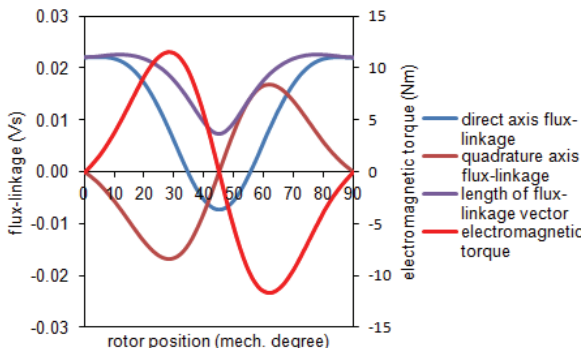


Fig. 4. Flux-linkage characteristics and electromagnetic torque characteristic in dependency on rotor position at RMS phase current of 100 A (rotor direct axis, stator MMF and magnetic axis of phase A are aligned for initial rotor position)

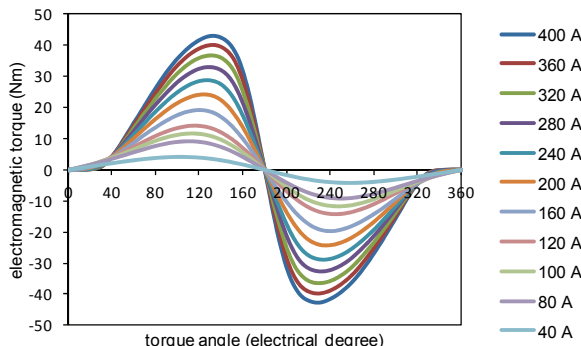


Fig. 6. Electromagnetic torque profile versus torque angle (angle between stator MMF and rotor direct axis) at different RMS values of stator current (phase current of 100 A correspond to current density of 6.33 A/mm² in stator slot conductor)

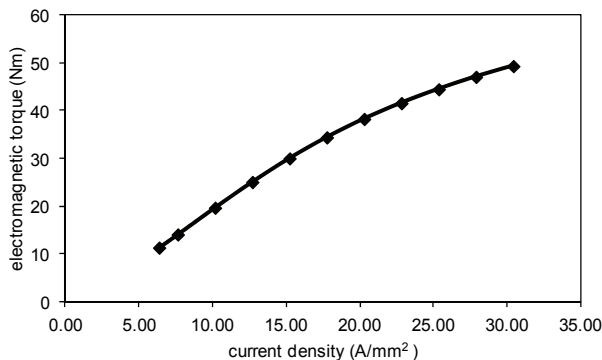


Fig. 8. Electromagnetic torque characteristic in dependency on current density (MTPA mode of operation)

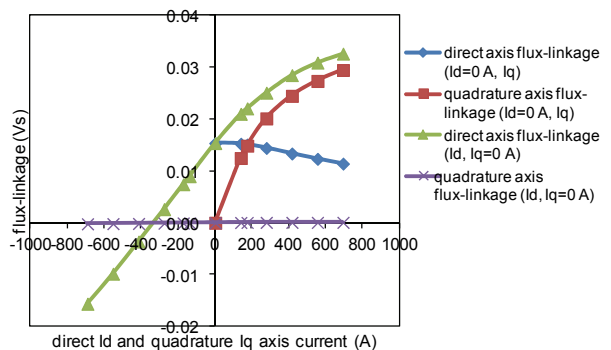


Fig. 3. Flux-linkage characteristics in dependency on direct and quadrature axis current

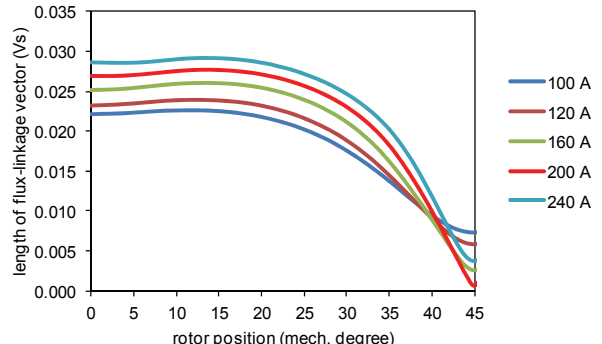


Fig. 5. Length of flux-linkage vector for different values of stator current in dependency on rotor position (rotor direct axis, stator MMF and magnetic axis of phase A are aligned for initial rotor position)

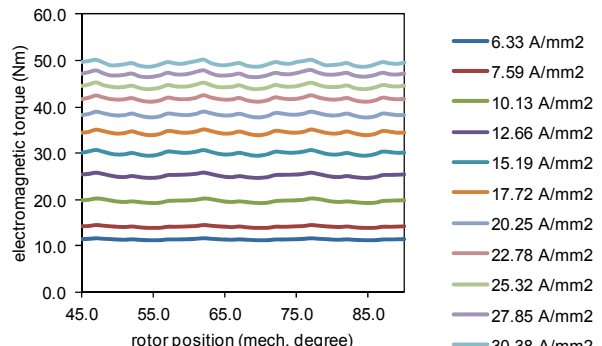


Fig. 7. Electromagnetic torque variation in dependency on rotor position at different RMS current densities in stator slot conductor (mode of operation: maximal torque per ampere (MTPA))

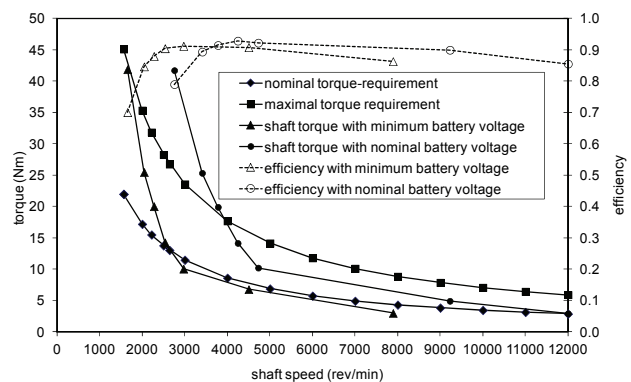


Fig. 9. Calculated torque characteristics in motor operation mode

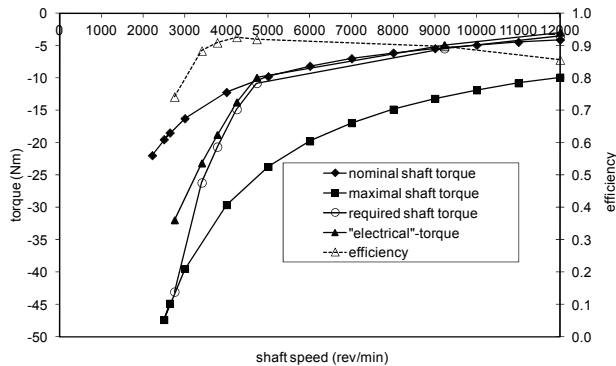


Fig. 10. Calculated torque characteristics in generator operation mode

For determination of machine thermal capability especially in the motor mode of operation the analytical approach has been used [5].

From the obtained results it is clear that the machine can operate at maximal torque requirements (40 Nm) only in short on/off cycles in order to prevent extensive heating of the machine. For nominal torque requirements (25 Nm) the maximal temperature in end winding region and magnet region does not exceed maximal allowed temperatures for continuous duty (ambient temperature 100 degree Celsius, inlet temperature of cooling media 80 degree Celsius, outlet temperature of cooling media 88 degree Celsius).

Conclusion

The results presented in the paper clearly show potential of the presented PM machine for belt-driven starter-generator applications. Future work will be dedicated to development of the appropriate control algorithm, building the prototype and experimental verification of the machine characteristics.

This work was supported in part by the Slovenian Research Agency, Project No. L2-1180.

REFERENCES

- [1] M. Barcaro et al., Performance evaluation of an integrated starter alternator using an interior permanent magnet machine, *IET Electr. Power Appl.*, 4 (2010), 539-546.
- [2] L. Alberti et al., IPM machine drive design and tests for an integrated starter alternator application, *IEEE Transactions on Industry Applications*, 46 (2010), 993-1001.
- [3] L. Chedot et al., Integrated starter generator: The need for an optimal design and control approach. Application to a permanent magnet machine, *IEEE Transactions on Industry Applications*, 43 (2007), 551-559.
- [4] J. G. Seo et al., Rotor-design strategy of IPMSM for 42 V integrated starter generator, *IEEE Transactions on Magnetics*, 46 (2010), 2458-2461.
- [5] J. Legranger et al., Combination of finite element and analytical models in the optimal multidomain design of the machines: application to an interior permanent magnet starter generator,

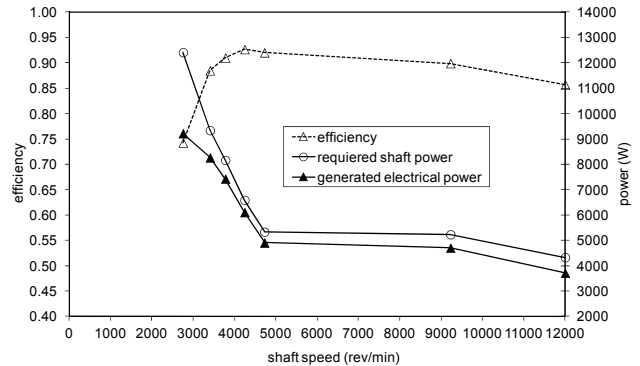


Fig. 11. Calculated power characteristic in generator operation mode

IEEE Transactions on Industry Applications 46 (2010), 232-239.

- [6] C. Feng et al., The performance research of starter-generator based on reluctance torque used in HEV, *IEEE Transactions on Magnetics*, 45 (2009), 635-638.
- [7] S. Chen et al., Design and testing of a belt-driven induction starter-generator, *IEEE Transactions on Industry Applications* 38 (2002), 1525-1533
- [8] K. Chwastek, Estimation method for the Jiles-Atherton model parameters-a review, *Przeglad Elektrotechniczny*, (2008), 145-148
- [9] J. Szczyglowski et al., Improvement of the prediction of the loss of magnetic material, *Przeglad Elektrotechniczny*, (2010), 45-47
- [10] M. Kuczmann, Measurement and simulation of vector hysteresis, *Przeglad Elektrotechniczny*, (2011), 103-106
- [11] M. Kuczmann, Vector Preisach hysteresis modelling: Measurement, identification and application, *Physica B-Condesed Matter*, 406 (2011), 1403-1409
- [12] B. Štumberger et al., Power and cooling capability of synchronous generator with interior permanent magnets: laboratory verification of machine characteristics, *Przeglad Elektrotechniczny*, 3 (2011), 183-186.
- [13] B. Štumberger et al., Determination of the adequate split ratio for high-efficiency permanent magnet synchronous motors with surface mounted magnets and concentrated non-overlapping windings , *Przeglad Elektrotechniczny*, 3 (2011), 187-189.
- [14] B. Štumberger et al., Analysis of iron loss in interior permanent magnet synchronous motor over a wide range of constant output power operation, *IEEE Transactions on Magnetics*, 36 (2000), 1846-1849
- [15] B. Štumberger et al., Design and finite-element analysis of interior permanent magnet synchronous motor with flux barriers, *IEEE Transactions on Magnetics*, 44 (2008), 4389-4392.
- [16] B. Štumberger et al., Accuracy of iron loss calculation in electrical machines by using different iron loss models, *Journal of Magnetism and Magnetic Materials*, 2003, (254/255), 269-271.

Authors: Bojan Štumberger, Miralem Hadžiselimović, University of Maribor, Faculty of Energy Technology, Hočevanjev trg 1, 8270 Krško, Slovenia,

E-mail: bojan.stumberger@uni-mb.si.